

Spontaneous lateral modulation in short-period superlattices investigated by grazing-incidence x-ray diffraction

O. Caha, P. Mikulík, and J. Novák

Institute of Condensed Matter Physics, Masaryk University, Kotlářská 2, 611 37 Brno, Czech Republic

V. Holý

Department of Electronic Structures, Charles University, Ke Karlovu 5, 121 19 Prague, Czech Republic

S. C. Moss

Department of Physics and Texas Center for Superconductivity and Advanced Materials, University of Houston, Houston, Texas 77204, USA

A. Norman and A. Mascarenhas

National Renewable Energy Laboratory, Golden, Colorado 80401, USA

J. L. Reno

Sandia National Laboratories, Albuquerque, New Mexico 87185-0601, USA

B. Krause

ESRF, BP 220, F-38043 Grenoble, France

(Received 9 March 2005; revised manuscript received 6 May 2005; published 8 July 2005)

The process of spontaneous lateral composition modulation in short-period InAs/AlAs superlattices has been investigated by grazing-incidence x-ray diffraction. We have developed a theoretical description of x-ray scattering from laterally modulated structures that makes it possible to determine the lateral composition modulation directly without assuming any structure model. From experimental intensity distributions in reciprocal space we have determined the amplitudes of the modulation and its degree of periodicity and their dependence on the number of superlattice periods. From the data it follows that the modulation process cannot be explained by bunching of monolayer steps and most likely, it is caused by stress-driven morphological instabilities of the growing surface.

DOI: [10.1103/PhysRevB.72.035313](https://doi.org/10.1103/PhysRevB.72.035313)

PACS number(s): 61.10.Dp, 68.65.La

I. INTRODUCTION

Processes of self-organization during the epitaxial growth of strained semiconductor heteroepitaxial systems represent a possible route for fabricating semiconductor quantum wires and dots (see Ref. 1, for a review). In a short-period superlattice grown nearly lattice-matched to a buffer layer underneath, such a process leads to a spontaneous modulation of the thicknesses of individual layers. A series of works has been devoted to a spontaneous modulation of InAs/AlAs superlattices grown on InAlAs buffer layers on InP(001) substrates.²⁻⁷ Transmission electron microscopy (TEM) revealed the dependence of the preferred modulation direction on the average stress in the superlattice; superlattices deformed in compression exhibit the lateral modulation along $\langle 100 \rangle$, while a deformation in tension leads to the modulation nearly along $\langle 310 \rangle$.^{6,8}

Theoretical description of the modulation process is based on two different models. If the crystallographic miscut of the substrate surface is large (above 1 deg), the density of monolayer steps on the vicinal surface is large. In this case a stress-induced bunching of the steps takes place^{1,9} creating a nearly periodic sequence of atomically flat terraces divided by bunches of monolayer steps. The resulting modulation is one-dimensional and the average direction of the bunches is

always perpendicular to the azimuthal direction of the miscut. If the miscut is small, the mean distance between the neighboring monolayer steps is larger than the diffusion length of the migrating adatoms. Then, the bunching process does not occur and the spontaneous modulation of the layer thicknesses is caused by a morphological instability of the growing surface—the Asaro-Tiller-Grinfeld instability (ATG).¹⁰ The direction of the modulation depends on the anisotropy of the physical properties (elastic constants, surface energy density) and usually a two-dimensional array of bumps is observed as a result of the ATG process. Several works have been published studying the ATG instability in superlattices.¹¹⁻¹⁴ In these papers, a continuum model was used based on a solution of a growth equation in a first-order approximation, assuming very small amplitudes of the surface corrugation. From the analysis of the stability of the solution of this equation, critical wavelength L_{crit} of the surface corrugation was found and its dependence on the material constants (surface energy, diffusivity of the adatoms, among others) was discussed.

In our previous works¹⁵⁻¹⁷ we have studied the structure of modulated InAs/AlAs superlattices by high-resolution x-ray scattering, namely by small-angle grazing-incidence x-ray scattering (GISAXS) and grazing-incidence diffraction (GID). In the case of samples with a large number of periods

(about 100) grown on a substrate with a large miscut of 2.5 deg we have found that the laterally modulated structure can be described as a result of bunching of monolayer steps. A detailed comparison of measured data with numerical simulations made it possible to determine the mean distances between the monolayer steps on the interfaces of such a modulated structure.

The aim of this paper is to study the *onset* of the modulation process by investigating a series of samples with various numbers of the periods, i.e., with various growth times. We investigate InAs/AlAs superlattices grown on substrates with nominally zero miscut; the superlattices are deformed in tension. We use the GID method for this purpose and we develop a theoretical description of x-ray scattering that makes it possible to determine the degree of the lateral modulation directly from the measured data without assuming any structure model.

The paper is organized as follows. In Sec. II we present the experimental data. In Sec. III we describe a theoretical procedure for the calculation of diffracted intensity; in Sec. IV we show a method of a direct analysis of experimental data without any *a priori* assumed structure model. Sections V and VI contain the analysis of experimental data.

II. EXPERIMENTAL RESULTS

We have investigated a series of four samples of InAs/AlAs superlattices grown by molecular beam epitaxy (MBE) on an InP(001) substrate covered by a 100 nm thick InAlAs buffer layer; the substrate was prepared without any nominal miscut. The samples have 2, 5, 10, and 20 superlattice periods; the InAs and AlAs thicknesses were nominally 1.9 monolayers (mL) in all samples. The chemical composition of the buffer layer was chosen so that the superlattices were slightly deformed in tension; for our samples, the critical thickness for plastic relaxation and creation of misfit dislocations is about $0.3 \mu\text{m}$, i.e., much larger than the superlattice thickness.¹⁸ The growth temperature was 535°C and the growth rate 0.5 mL/s . The details of the sample growth are published elsewhere.⁸

The x-ray measurements have been carried out at the beamline ID01 of the European Synchrotron Radiation Facility (ESRF, Grenoble). For all samples, we have measured the intensity distribution of the 400 and 040 diffraction in the $q_x q_y$ plane of the reciprocal space, i.e., parallel to the sample surface, at $q_z = \text{const}$. In order to enhance the surface sensitivity of the scattering and suppress the substrate signal, the angle of incidence of the primary beam was kept constant $\alpha_i = 0.27^\circ$, i.e., just below the critical angle of total external reflection ($\alpha_c = 0.28^\circ$) for the wavelength used ($\lambda = 1.5468 \text{ \AA}$).

In Fig. 1 we show the reciprocal space maps of all samples taken in diffraction 400, Fig. 2 compares the 400 and 040 reciprocal space maps of sample #20 (i.e., with 20 superlattice periods). In all cases except of the 2-period sample, the intensity distributions exhibit two side maxima in direction few degrees from $[100]$ and $[010]$ caused by the periodicity of the composition modulation, in addition to the central maximum (representing a coherent crystal truncation

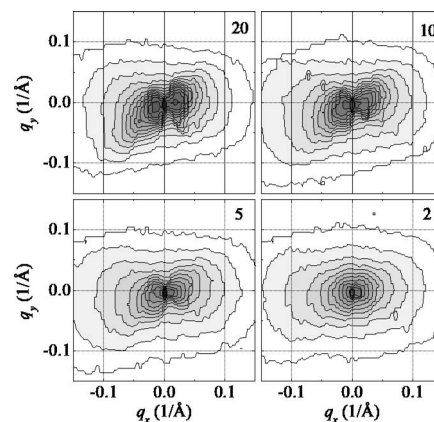


FIG. 1. The reciprocal space maps of sample #2–#20 of the diffracted intensity measured in diffraction 400. The diffraction vector is parallel to the q_x -axis, the numbers of the periods of the superlattices are denoted in the maps.

rod). From Fig. 1 it follows that with the increasing number of the superlattice periods, the intensity satellites are more pronounced, so that the lateral composition modulation becomes stronger. From the pair of the maps in 400 and 040 diffractions (Fig. 2) it follows that the sample is laterally modulated in two *orthogonal* directions making the angle of about $(12 \pm 3)^\circ$ with $\langle 100 \rangle$ directions, i.e., $(6 \pm 3)^\circ$ with the directions $[310]$ and $[\bar{1}30]$. Similar modulation was found previously for superlattices deformed in tension.^{6,8} In these works, however, the two modulation directions $[310]$ and $[130]$ were nonhogonal. The reason for this difference is not clear up to now, it might be caused by the fact that the samples in Refs. 6 and 8 have more than a hundred of periods. A more detailed analysis of the measured maps are presented in Sec. V.

III. THEORETICAL DESCRIPTION

In this section, we derive formulas describing the distribution of the diffracted intensity in a reciprocal plane ($q_x q_y$), i.e., $q_z = \text{const}$ parallel to the sample surface. Since, in a grazing-incidence geometry, both the incidence angle α_i and the exit angle α_f of the radiation are small, the vertical coordinate q_z of this reciprocal plane is much smaller than the distance $\Delta q_z = 2\pi/D$ of the superlattice satellites (D is the superlattice period). Therefore, for the purpose of the inten-

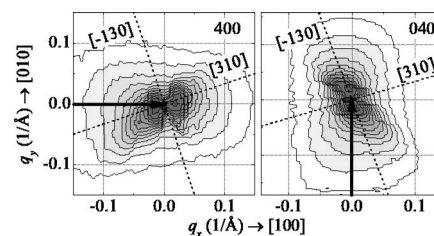


FIG. 2. The reciprocal space maps of sample #20 of the diffracted intensity measured in diffractions 400 and 040. The diffraction vectors are denoted by the arrows, the dotted lines represent the directions $[310]$ and $[\bar{1}30]$.

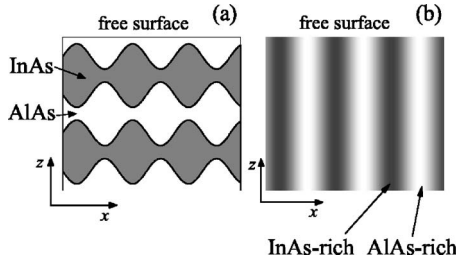


FIG. 3. The actual structure of a superlattice (a) is modeled by a vertically homogeneous layer in (b), its chemical composition periodically changes in a lateral direction.

sity calculation, the actual superlattice structure can be modeled by a single, vertically homogeneous layer. In this model, the lateral spontaneous modulation of the thicknesses of individual layers is represented by the lateral modulation of the chemical composition of this averaged layer, as shown in Fig. 3.

The amplitude of the wave scattered from the layer in a point $\mathbf{q}=(q_x, q_y, q_z)$ in reciprocal space is¹

$$E(\mathbf{q}) = A \sum_m F_m e^{-i\mathbf{q}\cdot\mathbf{r}_m} e^{-i\mathbf{h}\cdot\mathbf{u}_m}, \quad (1)$$

where the summation is performed over the unit cells of the layer, F_m is the structure factor of the unit cell in position \mathbf{r}_m , \mathbf{u}_m is its displacement vector and \mathbf{h} is the diffraction vector. The position vector \mathbf{q} in reciprocal space is $\mathbf{q}=\mathbf{Q}-\mathbf{h}$, where $\mathbf{Q}=\mathbf{K}_f-\mathbf{K}_i$ is the scattering vector, $\mathbf{K}_{i,f}$ are the wave vectors of the incident and scattered beams, respectively. Deriving Eq. (1) we have assumed the validity of the kinematical approximation and we have neglected the wave diffracted by the substrate underneath.

We denote c_m the concentration on the In atoms in the unit cell in position \mathbf{r}_m ; $c=\langle c_m \rangle$ is the average In content in the layer. In the layer assumed, the concentration c_m depends only on the in-plane coordinates (x_m, y_m) and not on the position z_m in direction perpendicular to the surface. The displacement vector \mathbf{u}_m is defined with respect to the averaged lattice of the layer corresponding to the mean In content c . The structure factor F_m is

$$F_m = (1 - c_m)F_{\text{AlAs}} + c_m F_{\text{InAs}} = \langle F \rangle (1 + \delta c_m \xi), \quad \delta c_m = c_m - c,$$

where F_{AlAs} and F_{InAs} are the structure factors of AlAs and InAs, respectively, $\langle F \rangle = (1 - c)F_{\text{AlAs}} + cF_{\text{InAs}}$ is the average structure factor, and $\xi = (F_{\text{InAs}} - F_{\text{AlAs}}) / \langle F \rangle$. In the following we assume that the modulation of the structure factor due to the chemical inhomogeneities is rather shallow, i.e., $\delta c_m \xi \ll 1$. Then

$$F_m \approx \langle F \rangle e^{\delta c_m \xi}. \quad (2)$$

Assuming linear elasticity, the displacement vector \mathbf{u}_m of the m th unit cell can be expressed by the formula

$$\mathbf{h} \cdot \mathbf{u}_m = \sum_n \delta c_n v_{mn}, \quad (3)$$

where the function v_{mn} contains the elastic Green function. Its form can be obtained by solving the equilibrium equation of linear elasticity

$$\frac{\partial \sigma_{jk}}{\partial x_k} + f_j = 0, \quad j, k = x, y, z, \quad (4)$$

where σ_{jk} is the stress tensor and f_j is the volume force density proportional to the local concentration $c_m \equiv c(\mathbf{r}_m)$ and to the lattice mismatch between InAs and AlAs. The details of the solution can be found elsewhere.^{16,17,19}

In this paper, we use a simplified form of function v_{mn} neglecting the surface relaxation of internal stresses. In this case, $v_{mn} \equiv v_{m-n}$ holds and the displacement vector u_m depends on $\mathbf{x}_m \equiv (x_m, y_m)$ only. From Eqs. (1) and (3) we obtain the following expression for the scattered amplitude

$$E(\mathbf{q}) = A \langle F \rangle \sum_m e^{-i\mathbf{q}\cdot\mathbf{r}_m} \exp\left(-i \sum_n \delta c_n p_{m-n}\right), \quad (5)$$

$$p_{m-n} = v_{m-n} + i\xi \delta_{mn},$$

δ_{mn} is the Kronecker delta.

In our model, the local concentration c_m is a random function of the in-plane position \mathbf{x}_m . The distribution of the scattered intensity in a plane $q_z = \text{const}$ averaged over a statistical ensemble of all sets of random values δc_m is

$$I(\mathbf{q}_{\parallel}) = B \sum_{m, m'} e^{-i\mathbf{q}_{\parallel}\cdot(\mathbf{x}_m - \mathbf{x}_{m'})} \left\langle \exp\left[-i \sum_n \delta c_n (p_{m-n} - p_{m'-n}^*)\right] \right\rangle, \quad \mathbf{q}_{\parallel} \equiv (q_x, q_y), \quad (6)$$

where the constant B contains a q_z -dependent term that is not affected by the lateral modulation of the layer.

The averaging in Eq. (6) can be performed using the cumulant expansion as follows.²⁰ We define

$$\left\langle \exp\left[-i \sum_n \delta c_n (p_{m-n} - p_{m'-n}^*)\right] \right\rangle \equiv e^{-T_{m-m'}} \quad (7)$$

and the function T can be expanded in the following cumulant series

$$T_{m-m'} = - \sum_{t=1}^{\infty} \frac{(-i)^t}{t!} \kappa_{m-m'}^{(t)}, \quad (8)$$

where $\kappa_{m-m'}^{(t)}$ is the t th cumulant. Restricting the cumulant series to the second cumulant only, we obtain

$$T_{m-m'} \approx \frac{1}{2} \kappa_{m-m'}^{(2)} = \frac{1}{2} \sum_{n, n'} \varepsilon_{n-n'} (v_{m-n} - v_{m'-n}) (v_{m-n'} - v_{m'-n'})$$

$$- 2i \text{Re} \xi \sum_n \varepsilon_n v_{m'-m+n} - |\xi|^2 \varepsilon_{m-m'}$$

$$- \text{Re}(\xi^2) \varepsilon_0 - 2 \text{Im}(\xi) \sum_n \varepsilon_n v_n, \quad (9)$$

where $\varepsilon_{m-m'} = \langle \delta c_m \delta c_{m'} \rangle$ is the correlation function of the fluctuations of the chemical composition.

In the following, we replace the discrete sums by integrals. The Fourier transformation of the function T is

$$\begin{aligned} T^{\text{FT}}(\mathbf{q}_{\parallel}) &= \int d^2(\mathbf{x}_m - \mathbf{x}_{m'}) T(\mathbf{x}_m - \mathbf{x}_{m'}) e^{-i\mathbf{q}_{\parallel} \cdot (\mathbf{x}_m - \mathbf{x}_{m'})} \\ &= \delta^{(2)}(\mathbf{q}_{\parallel}) T_c + T_{\text{diff}}^{\text{FT}}(\mathbf{q}_{\parallel}), \end{aligned} \quad (10)$$

the constant term

$$T_c = \int d^2\mathbf{q}'_{\parallel} \varepsilon^{\text{FT}}(\mathbf{q}'_{\parallel}) [(w^{\text{FT}}(\mathbf{q}'_{\parallel}))^2 - \text{Re}(\xi^2)]$$

appears only in a multiplicative pre-factor in the expression for the scattered intensity, and

$$T_{\text{diff}}^{\text{FT}}(\mathbf{q}_{\parallel}) = -\varepsilon^{\text{FT}}(\mathbf{q}_{\parallel}) |w^{\text{FT}}(\mathbf{q}_{\parallel}) + \xi|^2 \quad (11)$$

is the Fourier transformation of the diffuse part $T_{\text{diff}}(\mathbf{x} - \mathbf{x}')$ of the function $T(\mathbf{x} - \mathbf{x}')$. Here we have denoted $w^{\text{FT}}(\mathbf{q}_{\parallel}) = -iv^{\text{FT}}(\mathbf{q}_{\parallel})/a^2$, a is the averaged lateral lattice parameter of the layer.

The scattered intensity can be divided into two parts. The coherent part of the intensity is concentrated at the crystal truncation rod, i.e., this part is proportional to $\delta^{(2)}(\mathbf{q}_{\parallel})$. In the following, we will deal with the diffuse part of the scattered intensity

$$I_{\text{diff}}(\mathbf{q}_{\parallel}) = V \int d^2\mathbf{x} \int d^2\mathbf{x}' e^{-i\mathbf{q}_{\parallel} \cdot (\mathbf{x} - \mathbf{x}')} [e^{-T_{\text{diff}}(\mathbf{x} - \mathbf{x}')} - 1], \quad (12)$$

where V is a constant containing $\exp(-T_c)$, among others. Equations (11) and (12) will be used for the intensity calculation.

The correlation function $\varepsilon_{m-m'} \equiv \varepsilon(\mathbf{x}_m - \mathbf{x}_{m'}) = \langle \delta c_m \delta c_{m'} \rangle$ describes the random lateral modulation of the chemical composition of the layer. If the modulation were completely periodic, the correlation function could be expressed by means of a Fourier series

$$\varepsilon(\mathbf{x} - \mathbf{x}') = \sum_{\mathbf{G}} \varepsilon_{\mathbf{G}} e^{i\mathbf{G} \cdot (\mathbf{x} - \mathbf{x}')},$$

where \mathbf{G} are the vectors of a lattice reciprocal to the two-dimensional lattice of the composition modulation. In reality, the lateral modulation is not exactly periodic and it creates a disordered two-dimensional grid. Let us assume now that the lattice parameter $2\pi/L$ of this reciprocal lattice is randomly distributed (L is the period of the lateral composition modulation). Then the correlation function can be postulated in the form

$$\varepsilon(\mathbf{x} - \mathbf{x}') = \sum_{\mathbf{G}} \varepsilon_{\mathbf{G}} \chi_{\mathbf{G}}(\mathbf{x} - \mathbf{x}'), \quad (13)$$

where $\chi_{\mathbf{G}}(\mathbf{x}) = \int d^2\mathbf{G}' f_{\mathbf{G}}(\mathbf{G}') \exp(i\mathbf{G}' \cdot \mathbf{x})$ is the two-dimensional characteristic function of the random variable \mathbf{G}' and $f_{\mathbf{G}}(\mathbf{G}')$ is its distribution function around the reciprocal lattice point \mathbf{G} . Then the Fourier transformation $\varepsilon^{\text{FT}}(\mathbf{q}_{\parallel})$ of the correlation function equals:

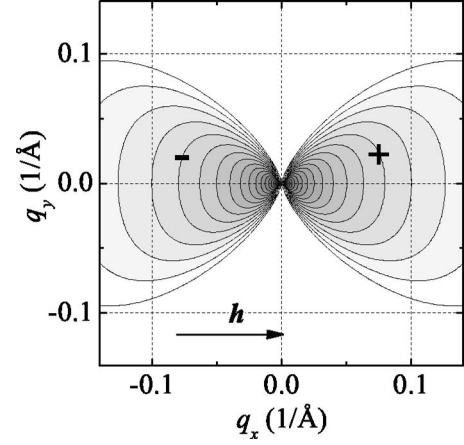


FIG. 4. The imaginary part of function $v^{\text{FT}}(\mathbf{q}_{\parallel})$ calculated in diffraction 400; the direction of the diffraction vector \mathbf{h} is denoted. The step of the contours is $10^{0.1}$, the positive (negative) lobe of the function is denoted by $+(-)$.

$$\varepsilon^{\text{FT}}(\mathbf{q}_{\parallel}) = 4\pi^2 \sum_{\mathbf{G}} \varepsilon_{\mathbf{G}} f_{\mathbf{G}}(\mathbf{q}_{\parallel}).$$

Since the distribution function $f_{\mathbf{G}}(\mathbf{G}')$ is normalized the integrated intensity of the \mathbf{G} th satellite of Fourier transformation $\varepsilon^{\text{FT}}(\mathbf{q}_{\parallel})$ does not depend on the degree of periodicity of the composition modulation and it equals $4\pi^2 \varepsilon_{\mathbf{G}}$. This integrated intensity is proportional to the product of the satellite height C with its full width at half maximum (FWHM) δq .

The explicit formula for the function v_{mm} occurring in the expression of the displacement field in Eq. (3) is complicated even for a material with cubic symmetry; however, a simple formula exists for its Fourier transformation:²¹

$$\begin{aligned} v^{\text{FT}}(\mathbf{q}_{\parallel}) &= -ia^2 \frac{\Delta}{|\mathbf{q}_{\parallel}|} (c_{11} + 2c_{12}) \left[\sum_{j=x,y} \frac{h_j q_j^0}{c_{44} + H(q_j^0)^2} \right] \\ &\times \left[1 + \sum_{j=x,y} \frac{c_{12} + c_{44}}{c_{44} + H(q_j^0)^2} (q_j^0)^2 \right]^{-1}. \end{aligned} \quad (14)$$

Here c_{11}, c_{12}, c_{44} are the elastic constants of a cubic material (in the 6×6 notation; we neglect the dependence of the elastic constants on the chemical composition), Δ is the lattice mismatch of pure InAs with respect of AlAs, a is the averaged in-plane lattice constant, $q_j^0 = q_j / |\mathbf{q}_{\parallel}|$, $j=x, y$, $\mathbf{h} = (h_x, h_y, 0)$ is the diffraction vector parallel to the sample surface, and $H = c_{11} - c_{12} - 2c_{44}$ is the elastic anisotropy factor ($H=0$ for an elastically isotropic continuum). Function $v^{\text{FT}}(\mathbf{q}_{\parallel})$ is purely imaginary and antisymmetric [$v^{\text{FT}}(-\mathbf{q}_{\parallel}) = -v^{\text{FT}}(\mathbf{q}_{\parallel})$]. Figure 4 shows the imaginary part of this function calculated in diffraction 400 (diffraction vector \mathbf{h} parallel to the q_x axis).

As an example, we calculate the functions $\varepsilon^{\text{FT}}(\mathbf{q}_{\parallel})$, $T_{\text{diff}}^{\text{FT}}(\mathbf{q}_{\parallel})$ and the resulting intensity distribution $I_{\text{diff}}(\mathbf{q}_{\parallel})$. We assume that the lateral inhomogeneities of the chemical composition create a disordered square lattice with the mean lattice parameter $\langle L \rangle = 340 \text{ \AA}$, the distance L was assumed randomly distributed with the Gamma distribution. Figure 5 shows the function Fourier transformation of the correlation

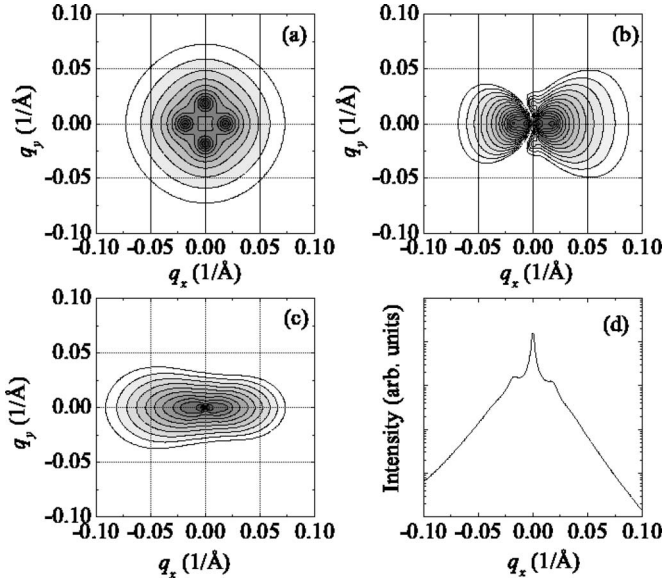


FIG. 5. The Fourier transformation $\varepsilon^{\text{FT}}(\mathbf{q}_{\parallel})$ of the correlation function of the lateral modulation (a) (the central δ -like peak is not shown), the Fourier transformation $T_{\text{diff}}^{\text{FT}}(\mathbf{q}_{\parallel})$ of the diffuse part of function $T(\mathbf{x}-\mathbf{x}')$ (b) and the resulting diffusely scattered intensity $I_{\text{diff}}(\mathbf{q}_{\parallel})$ (c). In panel (d), a cut of I_{diff} along q_x axis is plotted. The calculation has been performed for diffraction 400, the diffraction vector \mathbf{h} is parallel to the axis q_x .

function ε , the Fourier transformation of $T_{\text{diff}}(\mathbf{x}-\mathbf{x}')$, and the corresponding intensity distribution $I_{\text{diff}}(\mathbf{q}_{\parallel})$. In the correlation function in Fig. 5(a) we have neglected the central peak at $\mathbf{q}_{\parallel}=0$, since it has no influence on the shape of the resulting intensity distribution. The lateral modulation creates a disordered lattice along $[100]$ and $[010]$ creating only four satellites of the first order in the map of $\varepsilon^{\text{FT}}(\mathbf{q}_{\parallel})$; higher satellites disappear due to the disorder. The function $w^{\text{FT}}(\mathbf{q}_{\parallel})$ consists in two lobes (see Fig. 4) separated by a line of zero values (nodal line) perpendicular to \mathbf{h} ; therefore, in the function $T_{\text{diff}}^{\text{FT}}(\mathbf{q}_{\parallel})$ only the satellite maxima lying along $[100]$ are visible—see Fig. 5(d) (i.e., in the direction parallel to \mathbf{h}). The other two satellites are suppressed since they lie in the nodal line of w^{FT} . This is also the reason, why the resulting intensity distribution in Fig. 5(c) is elongated parallel to \mathbf{h} . The function $T_{\text{diff}}^{\text{FT}}$ is a coherent superposition of the antisymmetric function w^{FT} with a constant factor ξ . Since the two lobes of w^{FT} differ in sign, this superposition results in an asymmetry of function $T_{\text{diff}}^{\text{FT}}$ [Fig. 5(b)] and consequently in an asymmetric intensity distribution in Figs. 5(c) and 5(d). Therefore, the asymmetry in the intensity distribution in the radial direction (i.e., along \mathbf{h}) is a consequence of the interference of a wave scattered from the deformation field with a wave scattered from the inhomogeneities of the structure factor.

IV. DIRECT DETERMINATION OF THE CORRELATION FUNCTION ε FROM THE EXPERIMENTAL DATA

Formulas (11) and (12) make it possible to determine the correlation function $\varepsilon^{\text{FT}}(\mathbf{q}_{\parallel})$ directly from the measured data

without assuming any particular form of the correlation function $\varepsilon(\mathbf{x}-\mathbf{x}')$. The procedure consists in the following steps:

1. We calculate the inverse Fourier transformation of the intensity distribution $I(q_x, q_y) \equiv I(\mathbf{q}_{\parallel})$ (the Patterson function)

$$P(\mathbf{X}) = \frac{1}{4\pi^2} \int d^2\mathbf{q}_{\parallel} I(\mathbf{q}_{\parallel}) e^{i\mathbf{q}_{\parallel}\cdot\mathbf{X}}. \quad (15)$$

2. From the Patterson function we determine the diffuse part $T_{\text{diff}}(\mathbf{X})$ of the correlation function using the formula

$$T_{\text{diff}}(\mathbf{X}) = \ln[P(\mathbf{X})] + \text{const.}, \quad (16)$$

where the constant is determined so that

$$\lim_{|\mathbf{X}| \rightarrow \infty} T_{\text{diff}}(\mathbf{X}) = 0.$$

3. We calculate the Fourier transform

$$T_{\text{diff}}^{\text{FT}}(\mathbf{q}_{\parallel}) = \int d^2\mathbf{X} T_{\text{diff}}(\mathbf{X}) e^{-i\mathbf{q}_{\parallel}\cdot\mathbf{X}} \quad (17)$$

It is worthy to note that the resulting function $T_{\text{diff}}^{\text{FT}}(\mathbf{q}_{\parallel})$ is real. Knowing this function, using Eq. (11) we can directly determine $\varepsilon^{\text{FT}}(\mathbf{q}_{\parallel})$, since the function $w^{\text{FT}}(\mathbf{q}_{\parallel})$ and the factor ξ are known. The procedure fails in the points \mathbf{q}_{\parallel} , where $|w^{\text{FT}}(\mathbf{q}_{\parallel}) + \xi|^2$ is very small; this is the reason, why two diffractions (400 and 040, for instance) are necessary in order to reconstruct the correlation function $\varepsilon^{\text{FT}}(\mathbf{q}_{\parallel})$. We demonstrate the application of this method in the following section.

V. ANALYSIS OF MEASURED DATA

In this section we use the procedure described in the previous section to analyze the experimental data presented in Sec. II. In the measured maps in Figs. 1 and 2 only the side maxima lying on a line nearly parallel to \mathbf{h} are visible. The other pair of the maxima (on a line nearly perpendicular to \mathbf{h}) are suppressed, since the function $|w^{\text{FT}}(\mathbf{q}_{\parallel}) + \xi|^2$ is rather small here. The asymmetry of the maxima (the maximum at $q_x < 0$ is larger than that for $q_x > 0$) is caused by the interference of the contributions caused by the scattering from the strain field and from the chemical contrast.

From the maps in Fig. 2 we have calculated the Patterson function $P(\mathbf{X})$, the correlation function $T_{\text{diff}}(\mathbf{X})$, and its Fourier transformation $T_{\text{diff}}^{\text{FT}}(\mathbf{q}_{\parallel})$ (Fig. 6). A direct calculation of the correlation function $\varepsilon^{\text{FT}}(\mathbf{q}_{\parallel})$ from $T_{\text{diff}}^{\text{FT}}(\mathbf{q}_{\parallel})$ using Eq. (11) is not possible, since the division of $T_{\text{diff}}^{\text{FT}}(\mathbf{q}_{\parallel})$ by the function $|w^{\text{FT}}(\mathbf{q}_{\parallel}) + \xi|^2$ introduces a very large error in the points \mathbf{q}_{\parallel} , where this function is very small. However, in order to determine the degree of lateral modulation and its change during the superlattice growth, it is not necessary to extract $\varepsilon^{\text{FT}}(\mathbf{q}_{\parallel})$ from the measured data. Instead, we use the symmetric part $T_{\text{diff,sym}}^{\text{FT}}(\mathbf{q}_{\parallel})$ of $T_{\text{diff}}^{\text{FT}}(\mathbf{q}_{\parallel})$, plotted in Fig. 6(f); the lateral maxima of this function are nearly proportional to the maxima of $\varepsilon^{\text{FT}}(\mathbf{q}_{\parallel})$. In Fig. 7 we have plotted the functions $T_{\text{diff,sym}}^{\text{FT}}(\mathbf{q}_{\parallel})$ of all samples, extracted along the lines crossing the side maxima, with their fits by the pseudo-Voigt functions. Figure 8 demonstrates the dependences of the integrated amplitude $C\delta q$ (i.e., the area below the first satellite

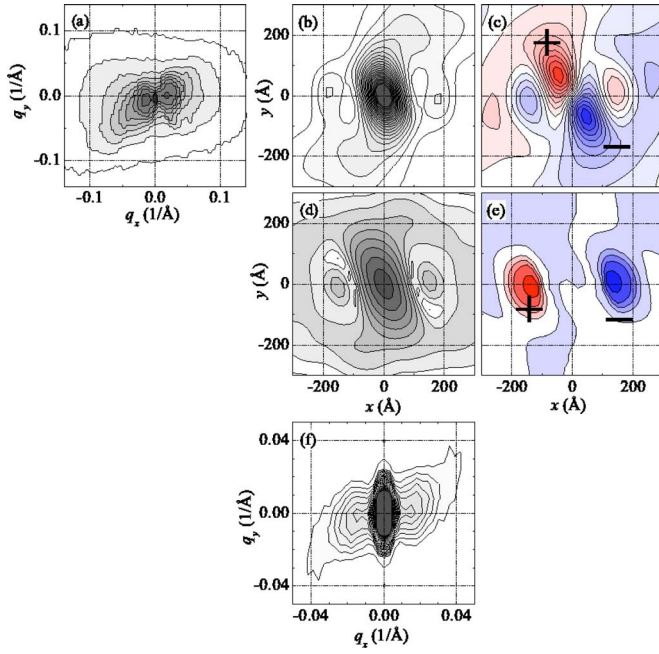


FIG. 6. (Color online) The reciprocal space maps of sample #20 of the diffracted intensity measured in diffractions 400 (a), the real part (b) and the imaginary part (c) of the Patterson function $P(\mathbf{X})$, the real part (d) and the imaginary part (e) of the function $T_{\text{diff}}^{\text{FT}}(\mathbf{X})$, and the symmetric part of the function $T_{\text{diff,sym}}^{\text{FT}}(\mathbf{q}_{\parallel})$ (f). In (c) and (e), the positive (negative) values are denoted by +(-); in the color version they are denoted by red (blue) colors, respectively.

maximum in $T_{\text{diff,sym}}^{\text{FT}}(\mathbf{q}_{\parallel})$ and width δq of the satellites on the number of superlattice periods, i.e., on the growth time. A scaling behavior of δq clearly visible. On the other hand, the period of the lateral modulation does not depend on the number of superlattice periods and from the positions of the lateral satellites the mean period of $\langle L \rangle = (267 \pm 15) \text{ \AA}$ follows.

VI. DISCUSSION

During the growth of a strained short-period superlattice, a spontaneous lateral modulation of the average chemical composition occurs. From our measurements it follows that

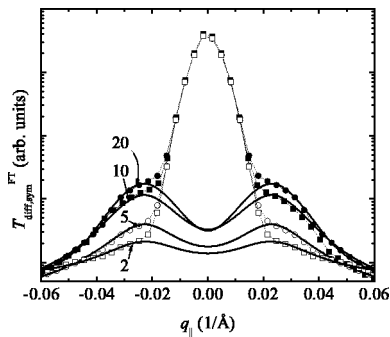


FIG. 7. The linear scans of the functions $T_{\text{diff,sym}}^{\text{FT}}(\mathbf{q}_{\parallel})$ of samples #2–#20 extracted along the line crossing the lateral intensity satellites (dots) along with their fits by the pseudo-Voigt function (lines).

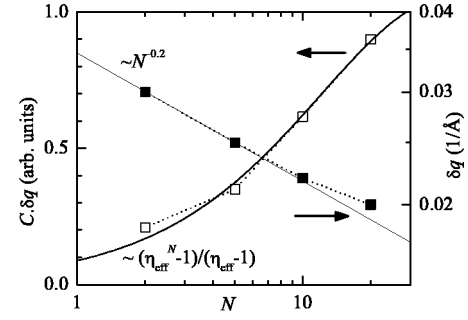


FIG. 8. The scaling behavior of the heights C and widths δq of the lateral satellites as functions of the number of the superlattice periods. Instead of the satellite heights C , the integrated satellite intensities $C\delta q$ are plotted.

the period of the modulation remains constant during the growth, the modulation amplitude increases and the periodicity of the modulation improves. The integrated amplitude $C\delta q$ of the lateral satellites of $T_{\text{diff,sym}}^{\text{FT}}$ is proportional to the ± 1 st Fourier coefficients of the correlation function $\varepsilon(\mathbf{x} - \mathbf{x}') = \langle \delta c(\mathbf{x}) \delta c(\mathbf{x}') \rangle$ of the local chemical composition. The integrated amplitude increases with the number N of the periods, while the width δq of the lateral satellites decreases with N as $N^{-0.2}$. From this behavior it follows that the first stages of the spontaneous modulation of the average chemical composition of a short-period super-lattice cannot be explained as a result of the bunching of monolayer steps at the interfaces. In the case of the step-bunching, the lateral period L of the modulation is always proportional to the mean number n_B of the monolayer steps in a bunch, i.e., to the modulation amplitude, so that the crystallographic miscut $\beta \approx n_B a / L$ remains constant (a is the lattice parameter).⁹

The results of this work indicating that the modulation period does not change with the number N of the superlattice periods, is in contradiction to our previous works,^{15–17} where we have found that the lateral composition modulation is caused by bunching of monolayer steps. In those works, however, we have investigated samples with a large intentional substrate miscut, i.e., with a large density of monolayer steps on the vicinal substrate surface. The samples in those works exhibited the lateral composition modulation only in one $[100]$ direction close to the azimuthal miscut direction, whereas two orthogonal modulation directions are present in the samples in this paper. This finding agrees with previously published results⁶ showing that the actual direction of the lateral composition modulation is affected by the miscut direction as well.

In our samples, the mechanism of the onset of the lateral modulation must be different. Most likely, this behavior can be ascribed to the Asaro-Tiller-Grinfeld instability,¹⁰ in which the critical wavelength of the surface corrugation,

$$L_{\text{crit}} = \frac{4\pi\gamma E}{3\sigma^2(1-\nu^2)} \quad (18)$$

depends on the stress σ in the growing layer, its surface energy γ , the Young modulus E , and the Poisson ratio ν . During the growth, the amplitude of the critical-wavelength

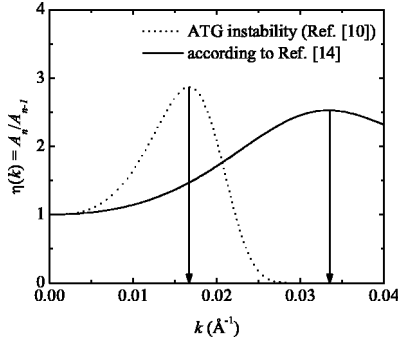


FIG. 9. The ratio $\eta(k)=A_n/A_{n-1}$ of the amplitudes of the interface corrugations at subsequent interfaces calculated for various wave vectors $k=2\pi/L$ of the surface corrugations using the ATG model (Ref. 10) and a multilayer model (Ref. 14). In the ATG model, we have assumed an InAs layer growing on InP. The arrows denote the critical wave vectors, corresponding to the critical wavelengths L_{crit} .

corrugation increases faster than other corrugation components and eventually, the only modulation period present on the growing surface is L_{crit} .

Using the numerical values of the material constants,²² we obtain $L_{\text{crit}} \approx 200 \text{ \AA}$ for a growing AlAs layer on InAs, and $L_{\text{crit}} \approx 380 \text{ \AA}$ for InAs on AlAs. These values roughly correspond to the obtained period L . In periodic multilayers, such an instability was investigated theoretically in Ref. 14; using this approach we obtain $L_{\text{crit}} \approx 200 \text{ \AA}$ for our samples. From this work it also follows that the predicted phases of the neighboring interfaces are opposite indeed, as assumed in our model in Fig. 3.

Using both theoretical models,^{10,14} one can calculate the ratio $\eta(k)=A_n/A_{n-1}$ of the amplitudes of the interface modulation of a given wave vector $k=2\pi/L$, in two subsequent interfaces of the same kind (InAs on AlAs, for instance). We have carried out these calculations for our samples and the results are in Fig. 9. The wave vector k , for which a maximum of $\eta(k)$ appears (arrows in Fig. 9) represents the critical interface corrugation wavelength L_{crit} ; within the ATG model this wavelength is given by Eq. (18). In Refs. 10 and 14, the surface development was investigated within a first-order approximation assuming very small amplitudes of the surface corrugation. Then, the ratio η remains constant during the growth and, therefore, the corrugation amplitude A_n exponentially increases. In reality, however, the limits of the first-order approximation are reached after the deposition of few superlattice periods, the exponential growth of the corrugation is inhibited and eventually a constant modulation amplitude is reached. Our structure model introduced in Fig. 3 assumes a constant corrugation amplitude; in order to account for a vertical profile of the modulation amplitude, we ascribe the determined modulation amplitude $C\delta q$ to be proportional to a weighted sum of the actual corrugation amplitudes

$$\sum_{n=1}^N A_n \exp[-b(N-n)] \sim \frac{\eta_{\text{eff}}^N - 1}{\eta_{\text{eff}} - 1},$$

since $A_n \sim \eta^n$. The factor $\exp[-b(N-n)]$ accounts for x-ray absorption ($b > 0$) and $\eta_{\text{eff}} \equiv \eta \exp(b)$. We have compared this function with the measured data in Fig. 8 and we found $\eta_{\text{eff}} \approx 0.9$. Since the theoretical value of η for the critical wavelength L_{crit} is larger than unity (see Fig. 9), the linear first-order approximation of the growth theory does not apply even in the very early stage of the growth.

In the theoretical description of the scattering process in Sec. III we have made two simplifications that do not affect the final results. Calculating the displacement field \mathbf{u}_m in Eq. (3), we have used a simplified form (14) of the function v_{mn} neglecting the surface relaxation of internal stresses. Another simplification consists in the assumption that the modulation of the structure factor F is shallow; this allowed us to express the structure factor in the form in Eq. (2). Both simplifications could influence the asymmetry for the intensities of the lateral satellites and they also affect the value $C\delta q$ of the modulation amplitude. However, in this paper we investigate only the relative changes of the amplitude and these changes remain unaffected by these simplifications. In order to determine the values of the modulation amplitude and not only its relative changes, both assumptions should not be made. This will be the subject of further investigations.

VII. SUMMARY

Using grazing-incidence x-ray diffraction, we have investigated the early stages of spontaneous lateral composition modulation during epitaxial growth of short-period superlattices InAs/AlAs on InP(001) substrates. From the analysis of experimental data it follows that the period of the modulation remains constant during the growth, while the modulation amplitude increases and the periodicity of the modulation improves. This behavior cannot be explained by bunching of monolayer steps and the modulation process is explained by the creation of periodic surface modulation (Asaro-Tiller-Grinfeld instability). A scaling behavior was found for the time evolution of the degree of periodicity of the composition modulation.

ACKNOWLEDGMENTS

This work is a part of the research program MSM 0021620834 that is financed by the Ministry of Education of the Czech Republic. The work has been partially supported also by the Grant Agency of the Czech Republic (project 202/03/0148). The synchrotron measurements have been carried out at the ID01 beamline, ESRF, Grenoble, the assistance of the beamline staff is appreciated. Sandia is a multi-program laboratory operated by Sandia Corporation, a Lockheed Martin Company, for the United States Department of Energy's National Nuclear Security Administration under Contract No. DE-AC04-94AL85000.

- ¹J. Stangl, V. Holý, and G. Bauer, *Rev. Mod. Phys.* **76**, 725 (2004).
- ²J. Mirecki Millunchick, R. D. Twesten, D. M. Follstaedt, S. R. Lee, E. D. Jones, Y. Zhang, S. P. Ahrenkiel, and A. Mascarenhas, *Appl. Phys. Lett.* **70**, 1402 (1997).
- ³D. M. Follstaedt, R. D. Twesten, J. Mirecki Millunchick, S. R. Lee, E. D. Jones, S. P. Ahrenkiel, Y. Zhang, and A. Mascarenhas, *Physica E (Amsterdam)* **2**, 325 (1998).
- ⁴A. G. Norman, S. P. Ahrenkiel, H. Moutinho, M. M. Al-Jassim, A. Mascarenhas, J. Mirecki Millunchick, S. R. Lee, R. D. Twesten, D. M. Follstaedt, J. L. Reno, and E. D. Jones, *Appl. Phys. Lett.* **73**, 1844 (1998).
- ⁵E. D. Jones, J. Mirecki Millunchick, D. Follstaedt, S. Lee, J. Reno, R. D. Twesten, Y. Zhang, and A. Mascarenhas, *Physica E (Amsterdam)* **2**, 44 (1998).
- ⁶A. G. Norman, S. P. Ahrenkiel, C. Ballif, H. R. Moutinho, M. M. Al-Jassim, A. Mascarenhas, D. M. Follstaedt, S. R. Lee, J. L. Reno, E. D. Jones, R. D. Twesten, and J. Mirecki-Millunchick, *Mater. Res. Soc. Symp. Proc.* **583**, 297 (2000).
- ⁷D. M. Follstaedt, J. L. Reno, E. D. Jones, S. R. Lee, A. G. Norman, H. R. Moutinho, A. Mascarenhas, and R. D. Twesten, *Appl. Phys. Lett.* **77**, 669 (2000).
- ⁸S. P. Ahrenkiel, A. G. Norman, M. M. Al-Jassim, A. Mascarenhas, J. Mirecki-Millunchick, R. D. Twesten, S. R. Lee, D. M. Follstaedt, and E. D. Jones, *J. Appl. Phys.* **84**, 6088 (1998).
- ⁹L. Bai, J. Tersoff, and F. Liu, *Phys. Rev. Lett.* **92**, 225503 (2004), and the citations therein.
- ¹⁰R. J. Asaro and W. A. Tiller, *Metall. Trans.* **3**, 1789 (1972); M. A. Grinfeld, *Sov. Phys. Dokl.* **31**, 831 (1986).
- ¹¹B. J. Spencer, P. W. Voorhees, and J. Tersoff, *Phys. Rev. B* **64**, 235318 (2001).
- ¹²P. Venezuela, J. Tersoff, J. A. Floro, E. Chason, D. M. Follstaedt, F. Liu, and M. G. Lagally, *Nature (London)* **397**, 678 (1999).
- ¹³L. E. Shilkrot, D. J. Srolovitz, and J. Tersoff, *Phys. Rev. B* **62**, 8397 (2000).
- ¹⁴Z.-F. Huang and R. C. Desai, *Phys. Rev. B* **67**, 075416 (2003).
- ¹⁵J. H. Li, V. Holý, Z. Zhong, J. Kulik, S. C. Moss, A. G. Norman, A. Mascarenhas, J. L. Reno, and D. M. Follstaedt, *Appl. Phys. Lett.* **78**, 219 (2001).
- ¹⁶J. H. Li, V. Holý, M. Meduňa, S. C. Moss, A. G. Norman, A. Mascarenhas, and J. L. Reno, *Phys. Rev. B* **66**, 115312 (2002).
- ¹⁷O. Caha, V. Krápek, V. Holý, S. C. Moss, J.-H. Li, A. G. Norman, A. Mascarenhas, J. L. Reno, J. Stangl, and M. Meduňa, *J. Appl. Phys.* **96**, 4833 (2004).
- ¹⁸J. W. Matthews and A. E. Blakeslee, *J. Cryst. Growth* **27**, 118 (1974).
- ¹⁹J. Novák, V. Holý, J. Stangl, Z. Zhong, G. Chen, and G. Bauer (unpublished).
- ²⁰S. Dietrich and W. Fenzl, *Phys. Rev. B* **39**, 8873 (1989).
- ²¹P. H. Dederichs and J. Pollmann, *Z. Phys.* **255**, 315 (1972).
- ²²The material parameters were taken from <http://www.ioffe.rssi.ru/SVA/NSM>. The surface energy was assumed 1 Jm^{-2} ; the surface diffusion constants were taken from <http://www.mse.ufl.edu/~spear>.